5
Control of Geometric Tolerances

5.1 INTRODUCTION

The wider adoption of CNC machine tools in manufacturing activities in recent years necessitated the application of Computer Aided Design and Manufacturing (CAD/CAM) software for tool-path generation, process parameter selection, cutting tool and fixture selection etc. The majority of commercial CAD/CAM software offers flexibility to regulate process parameters (for example, *ADOC*, *RDOC*, feed rate, etc.) and mode of milling (up or down milling) for controlling cutting forces and associated process faults. The tool-paths generated from CAD/CAM software do not account for process faults such as static deflections of end mills and thin-walled components that are commonly encountered during the end milling of thin-walled components. Therefore, these tool-paths cannot guarantee the conformance to dimensional or geometric tolerances specified by the designer. A number of approaches such as use of conservative cutting conditions [Stori and Wright, 2001], tool-path modification scheme [Dépincé and Hascoët, 2006], implementation of hardware for restricting the deflections [Watanabe and Iwai, 1983], development of cutting strategies for error control [Wang et al., 2017], etc. are proposed in the literature for the control of static deflections and dimensional error. It is realized in the previous chapter that the workpiece geometry, workpiece curvature and other parameters have a considerable influence on the geometric tolerance parameters. For example, the concave side machining experiences much higher cutting forces in comparison to convex or straight geometries for similar cutting conditions but geometric tolerances are much lower in this case. It is also realized that the thickness of a thin-walled component in an unmachined state can be used as a parameter to regulate rigidity and control of static deflections as well as geometric tolerances. It is imperative to develop an appropriate strategy to control static deflection-induced geometric tolerances during end milling of thin-walled components. This chapter presents a novel algorithm that modifies the localized thickness for the component generated at the end of roughing operation or semi-finished component such that the geometric tolerances for the finished component can be regulated within the desired tolerance specifications while performing the finish cutting sequence. The algorithm presented in this thesis work considers rigidity and nature of the thin-walled component at a given cutting instant as critical factors while designing the tool-path for optimum geometric tolerance parameters.

The present thesis proposes a novel Rigidity Regulation Approach (RRA) that derives the semi-finished workpiece geometry such that the geometric tolerances are controlled during the final machining pass or finish cutting sequence. The algorithm employs computational framework outlined in the previous chapter as a basis to determine representative semi-finishing geometries for thin-walled straight and circular components. The algorithm employs the PSO technique to estimate the semi-finishing workpiece geometry with regulated thickness along tool-path to control geometric tolerances within specific limits set by the designer. The proposed approach considers machining of thin-walled components in two phases; Firstly, generation of the semi-finished workpiece geometry having regulated thickness along the tool-path that offers desired geometric tolerances. Secondly, performing finish cutting sequence on the geometry obtained in the previous step using the contour-parallel tool-path. An overall algorithm for controlling geometric tolerances during end milling of thin-walled components is presented in

subsequent sections. The outcomes of the proposed model are substantiated further by conducting computational studies as well as machining experiments and results are presented subsequently.

5.2 RATIONALE FOR PROBLEM FORMULATION

Geometric tolerance is defined as an allowable deviation of the manufactured component from the desired geometry. The deviation in the form of tolerance zone is specified as a normal distance between two identical parallel features encompassing point cloud at the interface of the component and its environment. The tolerance zone is governed by three important elements namely, (i) size of the mating envelopes, (ii) orientation of the bounding feature and (iii) position of the reference feature. The detailed description of these elements in context of flatness and cylindricity can be found in Chapter 4. The subsequent subsections discusses the significance of these three individual elements while developing control strategies for the improved geometric tolerances during end milling of thin-walled components.

5.2.1 Size of Mating Envelopes

The size of the mating envelopes is defined as a distance of the reference feature from circumscribing and inscribing features bounding the farthest and nearest coordinates of the point cloud representing machined surface. The size of the mating envelopes for planar surface is computed as a normal distance of bounding planes from the reference plane, whereas in case of cylindrical surface it is defined as a radial distance of the bounding co-axial cylinders. The magnitude of tolerance zone is estimated as a difference in the size of mating envelopes determined from the distorted coordinate data representing machined surface. The present study considers thin-walled components as a candidate geometry with rigidity diminishing with the progress of material removal. The diminution of rigidity leads to inconsistent deflections along the length of cut as depicted in Figure 5.1a. As the component is constrained from the bottom and free to deflect from the other ends, deflections at free ends are considerably higher. Such inconsistency in the magnitude and profile of static deflections result into the increased spread of the coordinates and size of the mating envelope. The primary objective of the geometric tolerance minimization should be to regulate the magnitude and profile of deflections such that the spread of distorted coordinates is consistent along the length of cut as indicated in Figure 5.1b.

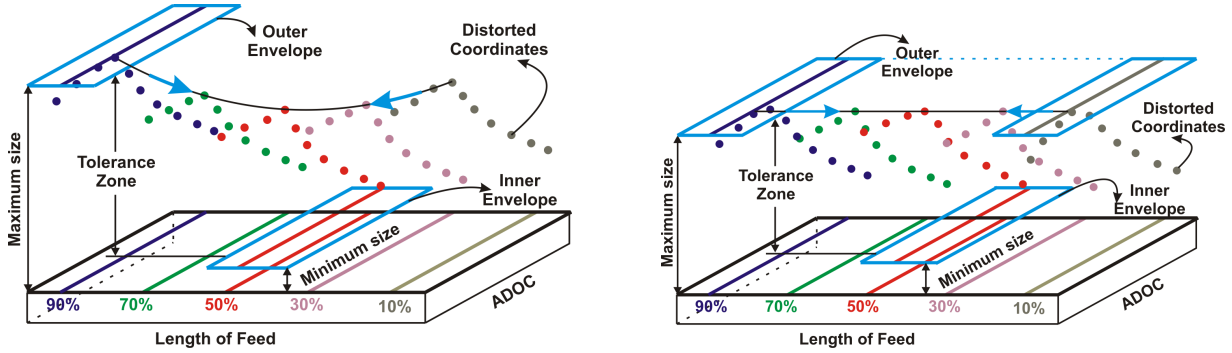

(a) Pre-Algorithm Implementation **(b)** Post Algorithm Implementation

Figure 5.1 : Illustration showing Size of Mating Envelope

5.2.2 Orientation of Bounding Feature

The orientation of a bounding feature is defined using the angular relationship of a manufactured component with reference to the desired or reference profile. The orientation is

evaluated as an inclination of the normal to parallel bounding planes for straight components while it is defined using axis inclination of two co-axial cylinders for cylindrical components. The orientation of the bounding feature using orientation requirements further modifies the tolerance zone as illustrated in Figure 5.2. The static deflections are considerably higher at free ends of the component (10% and 90% of the cut) in comparison to middle of the cut (50% of the cut) during end milling of thin-walled components. Figure 5.2b shows the interrelationship among feature orientation and magnitude of the tolerance zone for straight components. The orientation of bounding feature can be exploited to minimize the size of mating envelopes and accomplish the control of geometric tolerances. For example, deflection profiles and magnitudes along the length of cut can be adjusted to change the orientation considerably. The change of feature orientation increases the spread of distorted coordinates, but it can result into considerable improvement in the size of a tolerance zone. Therefore, the orientation of a bounding feature can be effectively employed to devise a strategy for achieving the tolerance zone with desired design specifications.

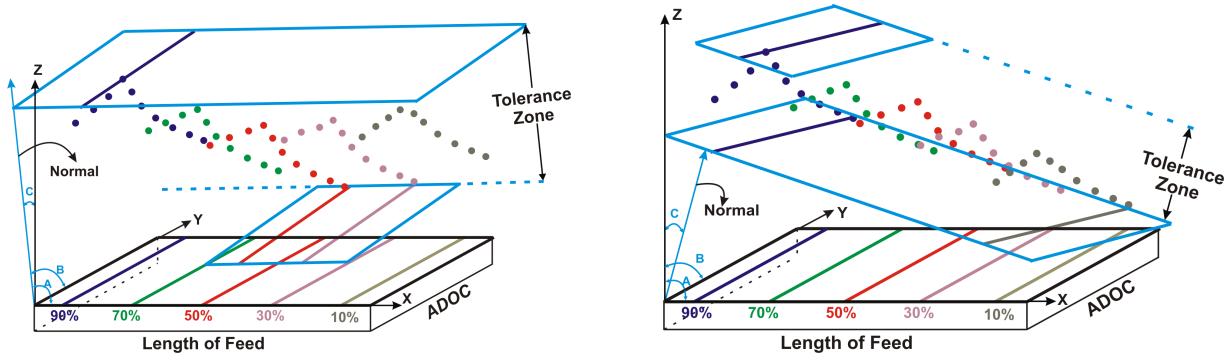

(a) Pre-Algorithm Implementation **(b)** Post Algorithm Implementation

Figure 5.2 : Illustration showing Orientation of Bounding Feature

5.2.3 Position of Reference Feature

The position of a reference feature is a datum from where sizes of mating envelopes are measured. It is evaluated as *Z*- intercept coordinates of the reference plane for straight components as shown in Figure 5.2. The position of a reference feature for cylindrical components is expressed using coordinates of a center point representing the axis of two coaxial cylinders. The reference position is critical for features such as pins, holes, slots, etc. that are part of an assembly where interchangeability requirements are important. The position of the reference for a bounding feature is illustrated using Figure 5.3a for representative cylindrical concave geometry. It can be realized that the location of maximum inscribing and minimum circumscribing cylinders are governed by the distorted point cloud at the end (90%) and middle (50%) locations of the cut respectively. Figure 5.3b shows the importance of the reference position in controlling the size of a tolerance zone for cylindrical concave geometries. It can be systematically manipulated by controlling the spread of deflected coordinates symmetrically along another center location for the coaxial cylinders. For example, the location of the point cloud deciding maximum inscribing and minimum circumscribing cylinders are swapped to the middle (50%) and end (90%) locations of the cut in Figure 5.3b. It is achieved by moving the center position of coaxial cylinders towards the middle of cut thereby controlling the magnitude of a tolerance zone.

The present thesis work devices an algorithm for controlling geometric tolerances by optimizing the values of these three elements. Based on the review of previous literature, it is realized that these three elements largely depend on the distribution of the point-cloud data representing the manufactured component. The distribution of distorted coordinates due

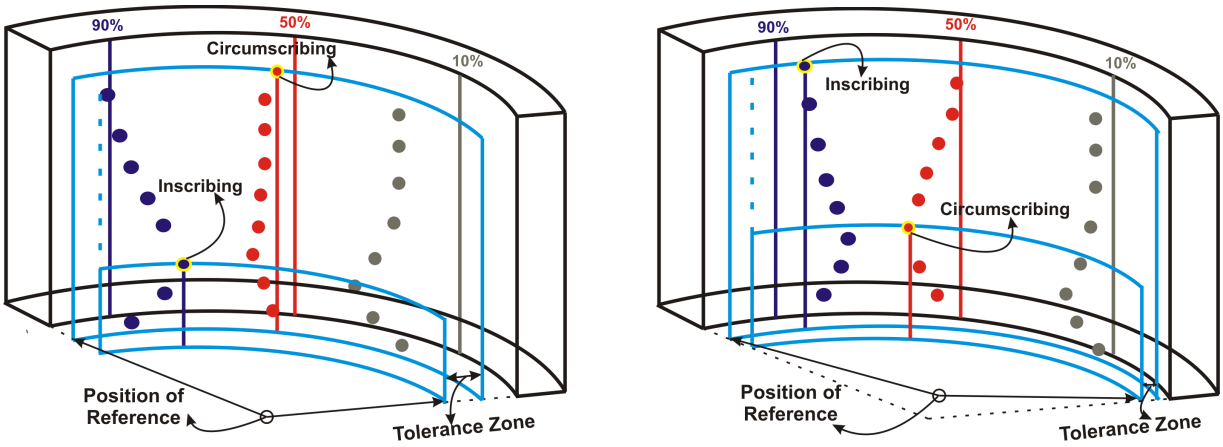

(a) Pre-Algorithm Implementation **(b)** Post Algorithm Implementation

Figure 5.3 : Illustration showing Position of Reference Feature

to static deflections of an end mill and thin-walled component is governed by two important factors namely, rigidity of the unmachined component and magnitude of cutting forces during the end milling operation. It was highlighted in the previous chapter that the thickness of component in an unmachined state thickness can be effectively exploited to control both these factors simultaneously. The RRA presented in this chapter employs the physics-based simulation approach to estimate unmachined component geometry to be obtained at the end of roughing operation such that the distribution of distorted point cloud data is optimized for control of geometric tolerance parameters.

5.3 RIGIDITY REGULATION APPROACH (RRA): ALGORITHM

The Rigidity Regulation Approach (RRA) aims to redistribute the material along length of thin-walled component such that the deflection magnitude or pattern generated during the finish cutting sequence is altered. The primary objective of the algorithm is to alter deflection patterns such that the geometric tolerance parameters for the finished component are optimized or maintained within the design limits. The algorithm considers thickness of thin-walled components as a governing parameter to regulate the rigidity of semi-finished geometry obtained at the end of roughing operation. The algorithm calculates pre-machined thickness to be achieved at different instants along length of the cut. The algorithm evaluates desired $RDOC$ (R_L) at different (L^{th}) cutting instants $(L = 1,2,3,.....,q)$ along the feed direction to achieve optimum geometric tolerance. The estimated $RDOC$ is added to the design thickness of the component to determine the profile of semi-finished geometry to be obtained at the end of roughing operation. The objective function can be formulated as Eq. 5.1

$$Estimate\ RM = [R_1, R_2, R_3, ...R_q]\ such\ that \tag{5.1}$$

$$Geometric\ Tolerance\ f(RM,\ ADOC,\ Feed\ rate)\ is\ Minimum$$

The approach aims to estimate $RDOC$ matrix (RM) by employing a meta-heuristic approach namely, Particle Swarm Optimization (PSO) algorithm. The step-wise procedure of implementing

RRA to determine redistribution of material on thin-walled components for optimum value of geometric tolerance parameters is outlined below. The algorithm is illustrated below using a representative example of thin-walled straight components. However, the algorithm is generic and it can applied to circular geometries with minor modifications. The algorithm is implemented subsequently to determine semi-finished workpiece geometries for both straight as well as circular geometries corresponding to optimum geometric tolerance parameters. The step wise procedure of implementing RRA for the optimization of geometric tolerance parameters is discussed subsequently.

Step 1 - Input Conditions: The algorithm commences by considering the final or desired geometric configuration of the thin-walled component expected by the designer as an input and it is depicted in Figure 5.4. The algorithm considers cutting parameters such as range of $RDOC$ ($RDOC_{max}$ and $RDOC_{min}$) for the regulation, $ADOC$, feed rate and number of sections along the length of cut $(L = 1, 2.3, ...q)$ as another set of input parameters.

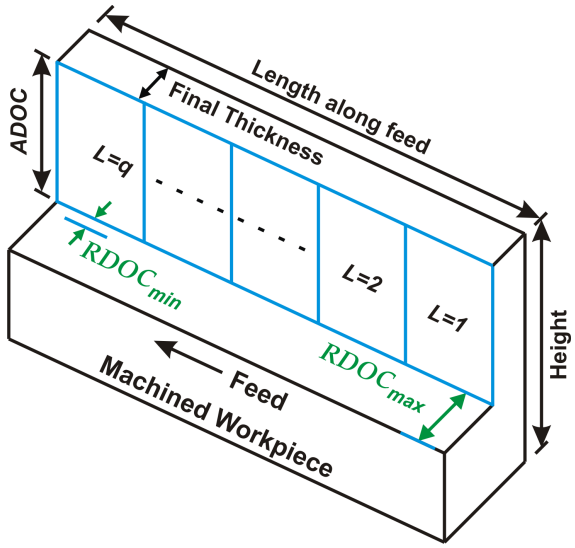

Figure 5.4 : Machined Configuration of the Workpiece

Step 2 - Initialization: The PSO algorithm considers m set of Radial Matrices $(RM^1, RM^2, RM^3, ..., RM^m)$ as a random possible solution termed as particles (l) $(l = 1, 2, 3, ..., m)$. Each particle is associated with the with random velocity matrices $(VM^1, VM^2, VM^3, ..., VM^m)$. The other parameters related to the PSO algorithm are defined subsequently e.g. bounding constraints for the variable ($[RDOC_{max}, RDOC_{min}]$), number of iterations (u) $(u = 1, 2, 3, ..., v)$, inertia weights (w_{max}, w_{min}), acceleration (c_1, c_2) and the termination condition.

Step 3 - Integration with Physics-based FE Model: The cutting geometry related parameters listed in Step 1 and radial matrices information along with other boundary conditions listed in Step 2 are input to develop FE models representing the thin-walled components corresponding to each particle in the PSO algorithm. Figure 5.5 depicts representative particles or solutions developed using integration of the PSO and FE model. The FE model of thin-walled components is meshed using 3-D 8-node solid shell elements (SOLSH 190) to facilitate the direct transfer of cutting forces as discussed in the Chapter 4. The cutting forces are estimated corresponding to the given cutting configuration using mechanistic cutting force model outlined in Chapter 3. The coordinates corresponding to each node in the transition zone are extracted for the application of cutting forces and static deflections are recorded at Surface Generation (SG) nodes.

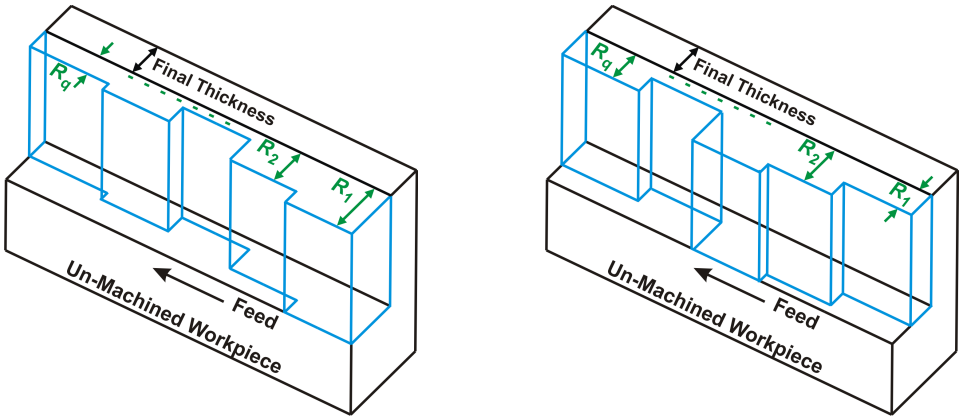

(a) Particle 1:
$RM^1 = [R_1^1, R_2^1, ..., R_q^1]$

(b) Particle 2:
$RM^2 = [R_1^2, R_2^2, ..., R_q^2]$

(c) Particle 3:
$RM^3 = [R_1^3, R_2^3, ..., R_q^3]$

(d) Particle m:
$RM^m = [R_1^m, R_2^m, ..., R_q^m]$

Figure 5.5 : Representative Workpiece Models corresponding to Particles

Step 4 - Realization of Candidate Solutions: The deflected coordinate data corresponding to the SG points represents distorted machined surface for each geometric configuration of the thin-walled component as outlined in Step 1. The distorted coordinates are input to the error estimation framework presented in the previous chapter to estimate geometric tolerance values and each set is termed as initial solution.

Step 5 - Finalizing Initial Solutions: The radial matrices $(RM^1, RM^2, RM^3, ..., RM^m)$ and geometric tolerance solution values $(GM^1, GM^2, GM^3, ..., GM^m)$ obtained for each particle are designated as the individual best set of *RDOC* combinations and chosen as a candidate solutions. The radial matrix corresponding to the lowest value of geometric tolerance parameters is designated as the global best set of *RDOC* combination among all candidate solutions obtained in Step 4.

Step 6 - Updating Solution Parameters: The velocity and radial matrices corresponding to each particle are updated according to the individual best and global best set of *RDOC* combination using Eqs. 5.2 - 5.4 respectively for obtaining candidate solutions for the subsequent iteration.

$$VM^{l}\,(u+1) = w(u)\,VM^{l}\,(u) + c_1\,r_1\,(LL_{best}\,(u) - RM^{l}\,(u)) + c_2\,r_2\,(GL_{best}\,(u) - RM^{l}\,(u)) \tag{5.2}$$

$$RM^{l}\,(u+1) = RM^{l}\,(u) + VM^{l}\,(u+1) \tag{5.3}$$

$$w(u) = (w_{max} - w_{min})\frac{(v-u)}{u} + w_{min} \tag{5.4}$$

Step 7 - Iteration Process: The computation process highlighted in steps 3-6 is repeated for obtaining geometric tolerance values and updated radial matrices. If the geometric tolerance value of any particle with the revised RM is lower than the individual best value during the previous iteration, the individual best set of $RDOC$ combination and tolerance value are replaced with the current RM. Similarly, if the lowest geometric tolerance value among all revised $(RM^1, RM^2, RM^3, ..., RM^m)$ is lower than the previous global best tolerance value, the global best set of $RDOC$ combination and tolerance value are replaced with the current radial matrix and its associated tolerance value of a particle.

Step 8 - Termination of the Solution Process: The algorithm repeats the computation process till the termination condition is satisfied. The present work employs the maximum number of iterations (v) as a termination criterion.

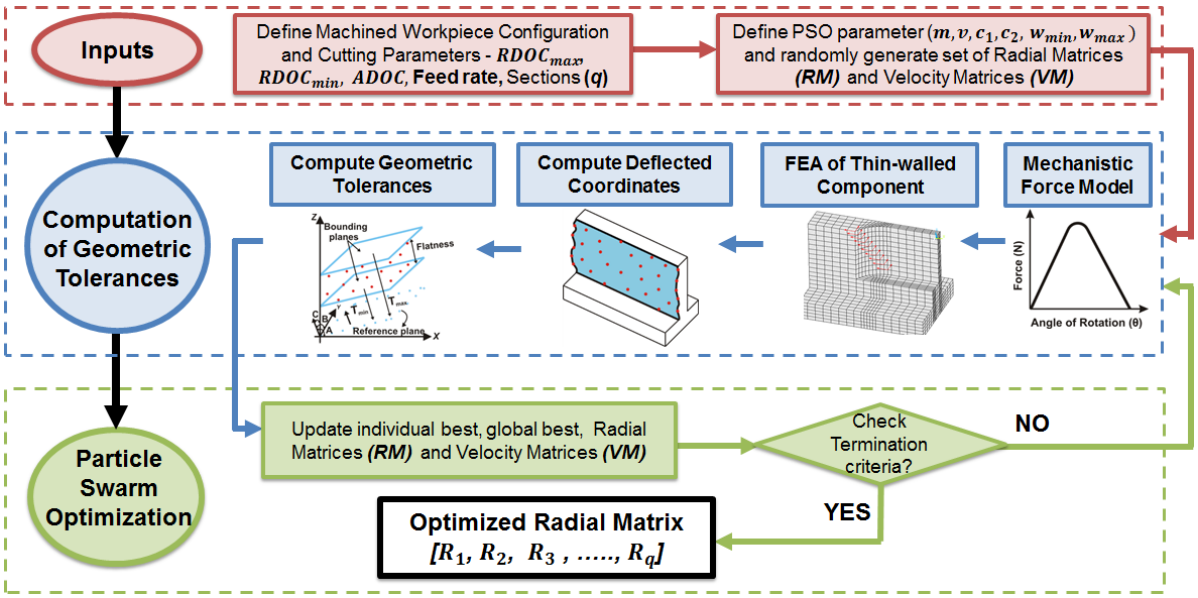

Figure 5.6 : Computational Framework for Rigidity Regulation Approach (RRA)

Figure 5.6 summarizes the step-wise procedure of determining optimized radial matrix using the RRA algorithm. The effectiveness of the PSO algorithm in determining the optimum solution depends on specific attributes such as the number of particles in a swarm, initial position of particles, inertia weights, and acceleration coefficients. The process of selecting the values of these parameters have been discussed in detail while employing PSO for estimating geometric tolerances in Chapter 4. The present chapter also employs similar process for selection of PSO parameters. The PSO-based rigidity regulation algorithm discussed in this section is implemented

in the form a computational tool to determine semi-finished thin-walled workpiece geometry that achieves the optimum geometric tolerance on the final component while performing finish cutting sequence.

5.4 COMPUTATIONAL AND EXPERIMENTAL RESULTS

The algorithm presented in the previous section is implemented as an integrated computational tool by combining MATLAB and ANSYS platforms to conceive the semi-finished workpiece geometry for representative thin-walled straight and circular components. The circular sections are analyzed for both concave and convex side machining to examine the effectiveness of proposed algorithm. Table 5.1 summarizes the dimensions of thin-walled component configuration for both straight as well as circular geometries, cutting tool specifications and process parameters used in the present study.

Table 5.1 : Workpiece Specification and Machining Conditions

Geometry	Radius (mm)		Final Component Thickness (mm)	$RDOC_{min}$ (mm)	$RDOC_{max}$ (mm)	$ADOC$ (mm)
	Inner	Outer				
Straight	–	–	2	1	4	25
Circular	39	41				
Machined Workpiece Dimension	: 100 x 50 x 2 (mm) (Length x Height x Thickness)					
Workpiece Material	: Aluminium 6061-T6					
Tool Material	: Solid Carbide (Kennametal - 4CH1600DK032A)					
Cutter Radius	: 8 mm					
Helix Angle	: 30°					
Number of Flutes	: 4					
Flute Length	: 32 mm					
Cutting Direction	: Down-cut					
Feed	: 300 mm/min					
Spindle Speed	: 2000 RPM					

The final thickness of the machined component is fixed at 2 mm for the consistency and comparison of results. The value of control variable *RDOC* is evaluated in the range of 1-4 mm (at 1 mm interval) along length of the component as depicted in Figure 5.5. The *ADOC* value is fixed as 25 mm for the effective utilization of an entire flute length of an end mill as per recommendation of the manufacturer. The computational algorithm initializes by dividing length of the thin-walled component into 10 equidistant locations (q) along length of the cut. The algorithm estimates the value of *RDOC* at each of these discrete locations to derive the semi-finished component geometry. The algorithm generates an offset geometry with variable thickness such that the optimum geometric tolerance parameters are obtained while performing finish cutting sequence using conventional contour parallel tool-path. The spline curve tool available in the CAD packages is employed to connect discrete *RDOC* locations determined along the tool-path to avoid a sudden change of the cutting configuration. The geometry obtained using the RRA algorithm is imported to the CAD/CAM package (Creo-Parametric) to obtain semi-finished configuration for the thin-walled component. The CAD model is imported to the APDL for conducting FE analysis and generation of point-cloud data representing distorted machined surface by employing computational framework discussed in the previous chapter.

A set of machining experiments are conducted on representative geometries to examine the efficacy of the proposed RRA in optimizing the geometric tolerance parameters. Firstly, the CAD model corresponding to the semi-finished workpiece geometry offering variable *RDOC*

during the finish cutting sequence is generated and imported into a CAM package to generate the part program for roughing operation. The part program generates the component geometry to be obtained at the end of roughing operation from the raw workpiece e.g. cuboid in this case. Secondly, a part program for the finish cutting sequence is generated for transforming the semi-finishing geometry into finished component as per the designer requirements. An additional set of CNC programs are also generated without considering RRA approach that generates contour parallel geometry at the end of roughing operation followed by a program to generate the component as per the designer requirement. The overall framework for end milling of thin-walled component with RRA and constant *RDOC* approach is presented in Figure 5.7. The part programs were input to the CNC Vertical Machining Center (AMS 540V) to generate semi-finished component geometries. The finish cutting sequences are performed using contour-parallel tool-path to obtain the final configurations of the thin-walled component for each case. The point-cloud data representing the actual machined surface is recorded using On-Machine Measurement setup (Renishaw OMP-40) depicted in Fig. 5.8. The subsequent subsections presents the analysis of results obtained from computational studies and machining experiments for straight and circular thin-walled components.

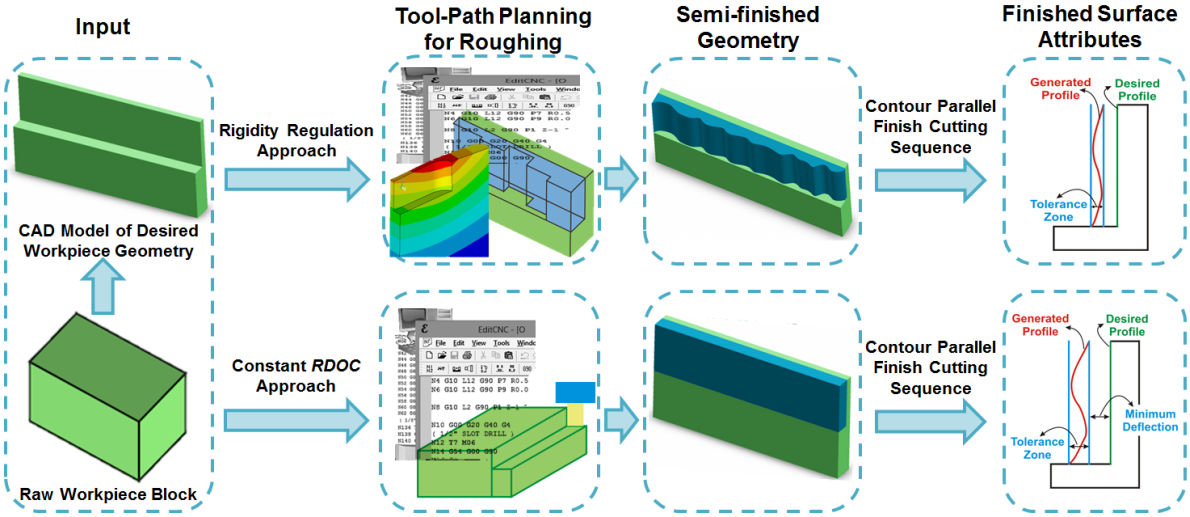

Figure 5.7 : Comparison of Rigidity Regulation Approach and Constant *RDOC* Approach

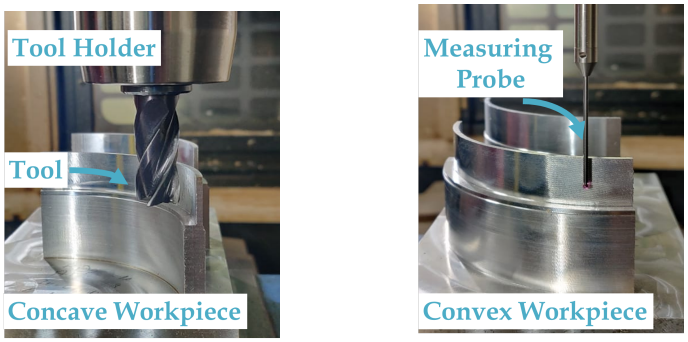

(a) Machined Component **(b)** Inspection Setup

Figure 5.8 : Machining and Inspection of Components after Finishing Pass

5.4.1 Algorithm Implementation for Straight Component

This section summarizes results of computational studies and machining experiments related to thin-walled straight components. The section assesses the effectiveness of proposed rigidity regulation approach in controlling geometric tolerances during milling of thin-walled straight components. Table 5.2 summarizes values of *RDOC* at different cutting locations along the length of thin-walled straight components obtained using RRA for candidate semi-finished geometry. The other variant of the thin-walled geometry considered for the comparison has constant *RDOC* along the length of component as commonly employed in the manufacturing industries.

Table 5.2 : Comparison of Geometric Tolerances for Straight Geometries

Approach	*RDOC* at q^{th} location along length of the component (start to end)	Flatness and Orientation Values	
		Computational	Experimental
Rigidity Regulation	1-1-2-3-3-4-4-4-4-4-4 (mm)	108.652 μm A = 90° 10′ 41″ B = 90° 05′ 20″	112.866 μm A = 90° 12′ 12″ B = 90° 04′ 05″
Constant *RDOC*	4-4-4-4-4-4-4-4-4-4-4 (mm)	157.830 μm A = 90° 14′ 07″ B = 90° 06′ 04″	161.519 μm A = 90° 08′ 24″ B = 90° 03′ 58″

The semi-finished workpiece geometry to be generated at the end of roughing operation using RRA with varying thickness and conventional geometry with constant thickness are shown in Figure 5.9a and 5.9b respectively. It can be seen that the component thickness is at a minimum level (1 mm) during the beginning of cut with gradual increase for the first half i.e. 0-50% of the cut. The RRA suggests maintaining the thickness at constant level for the remaining half i.e. 50-100% of the cut. The change of thickness and thereby *RDOC* results into the increase of cutting force from start to the middle of the cut. Meanwhile, the cutting force is expected to be at constant level from the middle to end of the cut as thickness is invariant. Such variation of cutting forces along the length of cut alters the deflection pattern thereby the spread of the coordinates. It can be realized that RRA seeks to reduce the rigidity and cutting forces during the first half of the cut while it consolidates rigidity and cutting forces during the subsequent part of the cut.

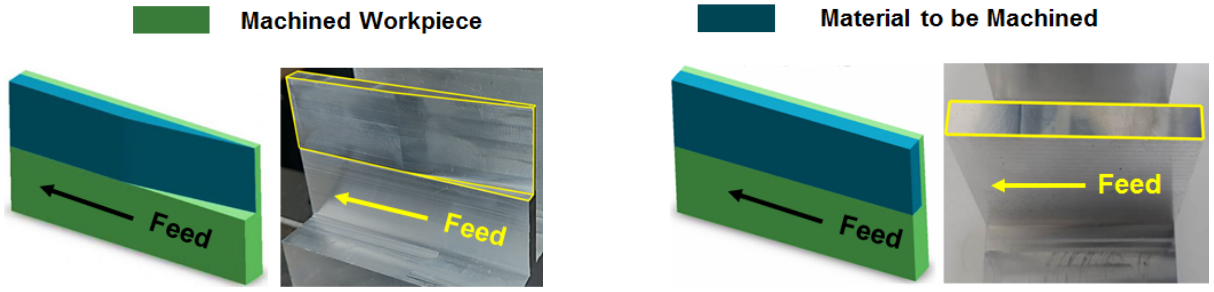

(a) With RRA Algorithm **(b)** With Constant *RDOC*

Figure 5.9 : Semi-finished Configuration of Straight Component

Figure 5.10a and 5.10b depicts the variation of distorted coordinates along length of the thin-walled straight component while performing finish cutting sequence on semi-finished geometries obtained through RRA and constant *RDOC* approach. It can be seen that the magnitude of distortion increases from the start to the end of the cut when finish cutting sequence is performed on the geometry obtained using RRA. This is in contrast to the distortion data obtained while

performing finish cutting sequence on the component geometry with constant *RDOC* that involves higher deflections towards ends of the cut compared to the middle section. The reduction in the magnitude of distortion during the initial half of the cut for RRA can be attributed to the lower magnitude of *RDOC* and cutting forces. It can be seen that the band of distorted coordinates representing width of the tolerance zone or flatness value is considerably narrowed upon implementation of the RRA. Table 5.2 summarizes the comparison of flatness error obtained through the RRA and constant *RDOC* approach. It can be seen that the flatness error estimated using computational model is in good agreement with experimentally measured values.

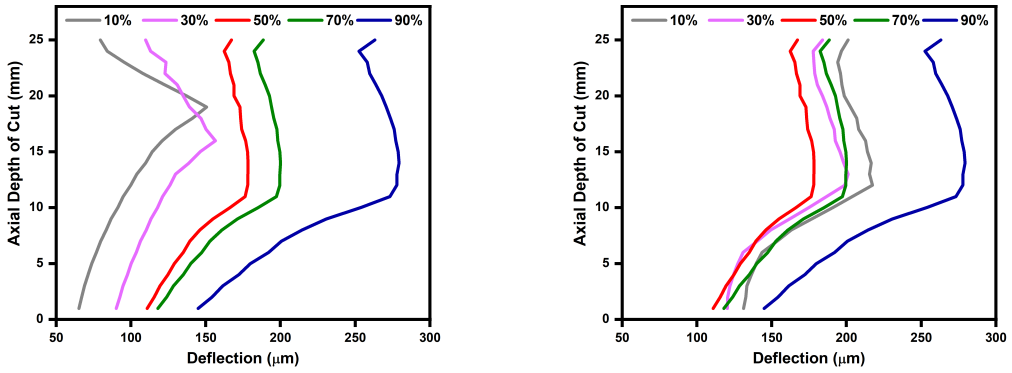

(a) With RRA Algorithm **(b)** With Constant *RDOC*

Figure 5.10 : Axial Surface Error Variation along Length of Component for Straight Component

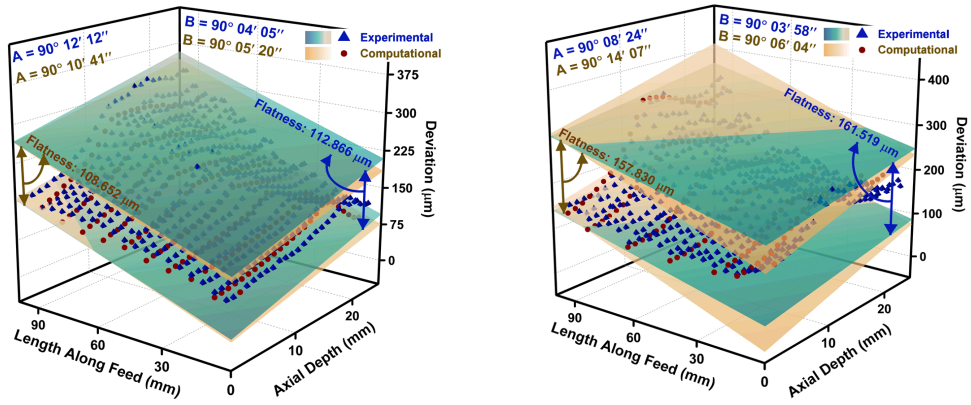

(a) With RRA Algorithm **(b)** With Constant *RDOC*

Figure 5.11 : Flatness Profile and associated Parameters for Straight Component

Figure 5.11a and 5.11b depicts the graphical representation of machined surface and flatness parameters obtained using RRA and constant *RDOC* approach along with the experimental results. The flatness error is considerably reduced upon implementation of the RRA although the magnitude and location of maximum distortion is identical in both cases. This was further investigated by analyzing another parameters of the geometric tolerance namely orientation of the bounding feature subsequently in controlling the width of a tolerance zone. It can be seen that the increased magnitude of distorted coordinates from the start to the end of the cut reduces width of the tolerance zone and flatness error by regulating orientation of the bounding planes. The change of orientation for the bounding planes in reducing the flatness error was captured effectively by the computational models and the same is summarized in Table 5.2.

5.4.2 Algorithm Implementation for Circular Concave Components

This section summarizes the results of computational studies and machining experiments related to thin-walled circular components while machining from the concave side. The section assesses the effectiveness of the proposed approach in controlling geometric tolerances during the milling of thin-walled circular concave components. Table 5.3 summarizes the values of *RDOC* at different locations along the length of thin-walled circular concave component obtained using RRA for the semi-finished geometry. The *RDOC* values are subtracted from the radius of the desired workpiece configuration at respective locations to obtain the semi-finished component geometry. The other variant of the thin-walled geometry with constant *RDOC* along the length of component is considered for the comparison as commonly employed in the manufacturing industries.

Table 5.3 : Comparison of Geometric Tolerances for Circular Concave Component

Approach	*RDOC* at q^{th} location along length of the component (start to end)	Cylindricity and Reference Value	
		Computational	Experimental
Rigidity Regulation	4-3-2-1-1-1-1-2-3-4 (mm)	62.75 μm X = 96.682 Y = 126.564	75.58 μm X = 101.427 Y = 130.970
Constant *RDOC*	4-4-4-4-4-4-4-4-4-4 (mm)	88.33 μm X = 34.615 Y = 20.230	103.36 μm X = 41.290 Y = 28.762

The semi-finished workpiece geometries obtained at the end of roughing operation using RRA with varying thickness and a conventional geometry with constant thickness are shown in Figure 5.12a and 5.12b respectively. It can be seen that the RRA considers maintaining *RDOC* at maximum level (4 mm) at the beginning (0-10%) and end (90-100%) of the cut. The RRA considers the gradual reduction of the thickness from the start to middle section of the cut (40-60%) to reach the minimum value (1 mm). The thickness increases gradually from the middle (50% of the cut) of the component to end (90% of the cut) resulting into increased rigidity to resist elevated cutting forces. The change of thickness results into higher rigidity accompanied with elevated cutting force towards the beginning and end of the cut. The middle section has lower rigidity and it will be subjected to the smaller magnitude of cutting forces. The variation of the rigidity and cutting forces along the length of thin-walled component alters the deflection pattern thereby the spread of the distorted coordinates.

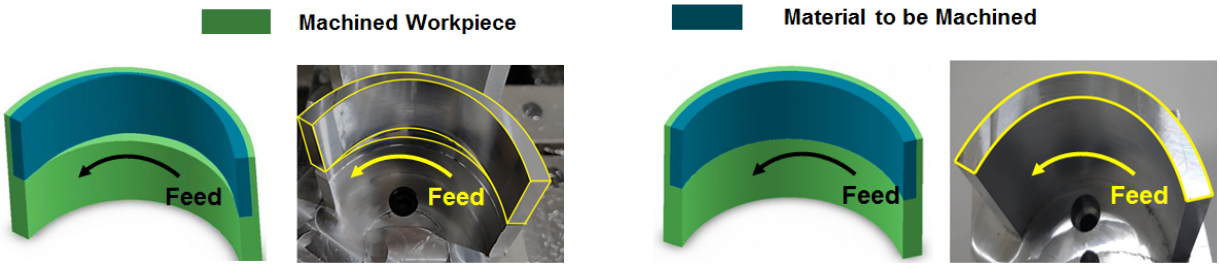

(a) With RRA Algorithm **(b)** With Constant *RDOC*

Figure 5.12 : Semi-finished Configuration of Circular Concave Component

Figure 5.13a and 5.13b depicts the variation of distorted coordinates at different locations along the length of thin-walled circular concave component while performing finish cutting

sequence on semi-finished geometries obtained through both approaches. It can be seen that the magnitude of distortion reduces considerably at the middle portion of the cut when finish cutting sequence is performed on geometries obtained using RRA in comparison to the constant *RDOC* approach. The reduced distortions at the middle portion of the cut can be attributed to the lower cutting forces with cutting portion located farther from the free ends. The distortions at the beginning and end of the cut for both approaches are similar due to identical cutting configuration. It is also evident that the overall magnitude and variation within the axial error profile increases along the length of cut for geometries obtained using RRA. Meanwhile, such behaviour is not observed for geometries obtained using constant *RDOC* approach where the ends show considerably higher magnitude of distortion with higher variation within axial error profile. Table 5.3 summarizes the comparison of cylindricity error obtained through the RRA and constant *RDOC* approach. It can be seen that the cylindricity error estimated using computational model is in good agreement with experimentally measured values.

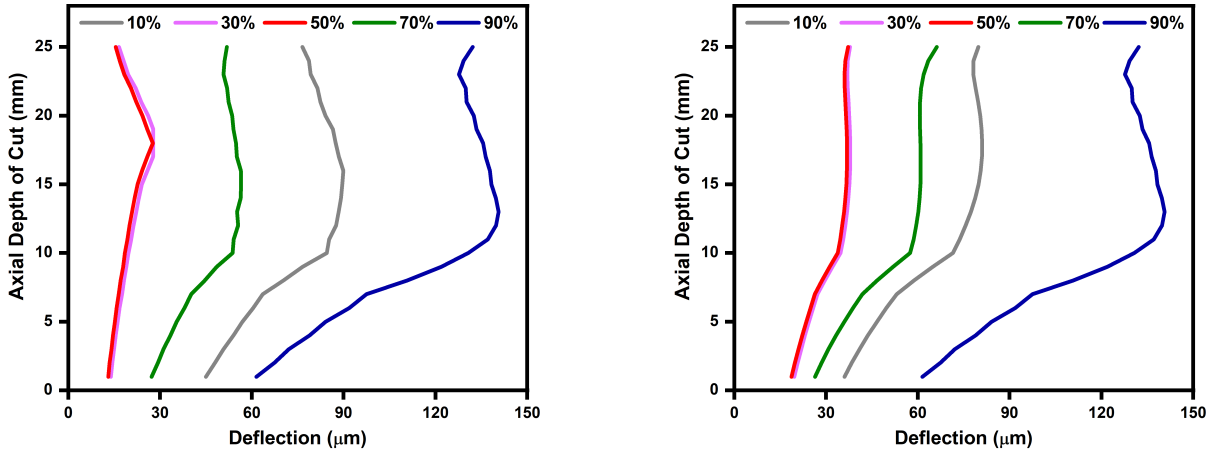

(a) With RRA Algorithm **(b)** With Constant *RDOC*

Figure 5.13 : Axial Surface Error Variation along Length of Component for Circular Concave Component

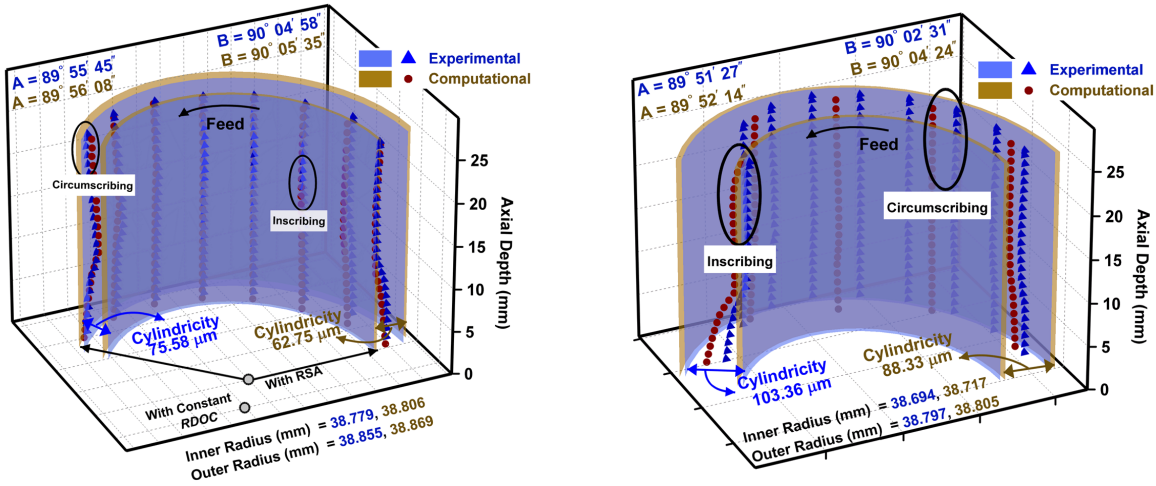

(a) With RRA Algorithm **(b)** With Constant *RDOC*

Figure 5.14 : Cylindricity Profile and associated Parameters for Circular Concave Component

Figure 5.14a and 5.14b depicts the graphical representation of machined surface as well as cylindricity parameters obtained using RRA and constant *RDOC* approach along with the experimental results. The cylindricity error is considerably lower when RRA is implemented to obtain the semi-finished geometry in comparison to the constant *RDOC* approach. The results are in contrast to the general comprehension which expects tolerance zone to increase due to wider spread and larger magnitude of distorted coordinates obtained with RRA. The improvement of the tolerance zone can be attributed to the change in position of reference feature for the distorted data that assist in minimizing the tolerance zone. The RRA seeks to reposition the center of coaxial cylinders towards middle section of the cut such that deflected coordinates at 30-60% of the cut governs the inscribing cylinder, while deflected coordinates at 90% of cut governs the circumscribing cylinder. The modified center location of coaxial cylinders was captured effectively through the computational and experimental results which is summarized in Table 5.3. It is important to note that the displaced center position must accord to the other tolerancing parameters such as position tolerance and material condition (MMC or LMC).

5.4.3 Algorithm Implementation for Circular Convex Components

This section summarizes the results of computational studies and machining experiments related to thin-walled circular components while machining from the convex side. The section assesses the effectiveness of the proposed approach in controlling geometric tolerances during end milling of thin-walled circular convex components. Table 5.4 summarizes the values of *RDOC* at different cutting locations along the length of thin-walled circular convex components obtained using RRA as a candidate semi-finished geometry. The *RDOC* values are added to the radius of the desired workpiece geometry at the corresponding locations to obtain the semi-finished configuration of the component. The other variant of the semi-finished geometry consisting of constant *RDOC* along the length of component as commonly employed in the manufacturing industries.

Table 5.4 : Comparison of Geometric Tolerances for Circular Convex Component

Approach	*RDOC* at q^{th} location along length of the component (start to end)	Cylindricity and Radius Values	
		Computational	Experimental
Rigidity Regulation	1-2-3-4-4-4-4-3-2-1 (mm)	59.52 μm Inner = 41.076 mm Outer = 41.135 mm	70.98 μm Inner = 41.092 mm Outer = 41.163 mm
Constant *RDOC*	4-4-4-4-4-4-4-4-4-4 (mm)	83.16 μm Inner = 41.123 mm Outer = 41.206 mm	91.82 μm Inner = 41.112 mm Outer = 41.204 mm

The semi-finished workpiece geometries to be obtained at the end of roughing operation using RRA having varying thickness and a normal geometric configuration with the constant thickness are shown in Figure 5.15a and 5.15b respectively. It can be seen that the thickness is maintained at a minimum level (1 mm) at the start (0-10%) and end (90-100%) of the cut. The thickness value gradually increases from the start to middle section of the cut and attains maximum value of 4 mm at 40-60% of the cut. The change of thickness results into lower rigidity accompanied with the reduced cutting forces towards the beginning and end of the cut. The middle section has higher rigidity due to increased thickness but it experiences more cutting forces. The thickness gradually reduces from the maximum value at the middle (50% of the cut) to the minimum level at the end of cut resulting into exactly opposite variation of cutting forces and rigidity during this period. Such variation of the rigidity and cutting forces at different location along the length of component effects the deflection pattern and the spread of the distorted coordinates.

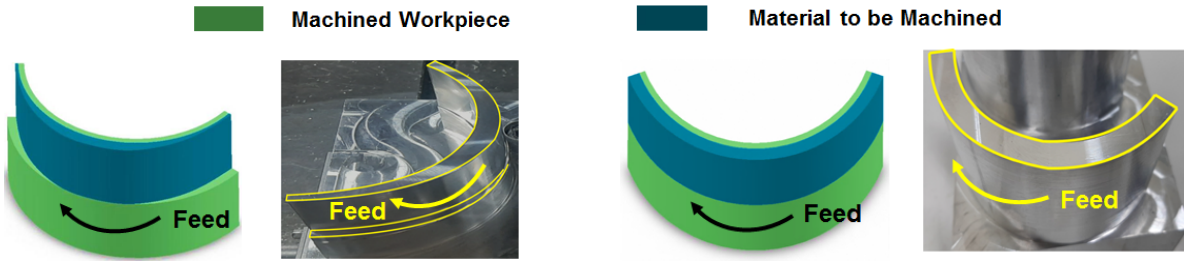

(a) With RRA Algorithm **(b)** With Constant *RDOC*

Figure 5.15 : Semi-finished Configuration of Circular Convex Component

Figure 5.16a and 5.16b depicts the variation of distorted coordinates at different locations along the length of thin-walled circular convex component while performing finish cutting sequence on semi-finished geometries obtained using both approaches. It can be seen that the magnitude of distortion reduces during the beginning and end of the cut for the semi-finished geometry obtained using RRA in comparison to constant *RDOC* components. The reduction in the magnitude of distortion at the beginning and end of the cut can be attributed to the lower magnitude of *RDOC* and cutting forces. The static deflections remain identical at the middle of the cut for geometries obtained using both approaches as cutting configuration is similar. It is realized that the regulation of local workpiece rigidity and cutting forces with the progress of cut affects the profile and magnitude of workpiece distortion significantly. The RRA manages to reduce the spread of the distorted coordinates by redistributing workpiece material to manipulate local rigidity of the component. Table 5.4 presents the summary of cylindricity parameters obtained through the RRA and constant *RDOC* approach. It can be seen that the results estimated using computational models are in good agreement with experimentally measured values.

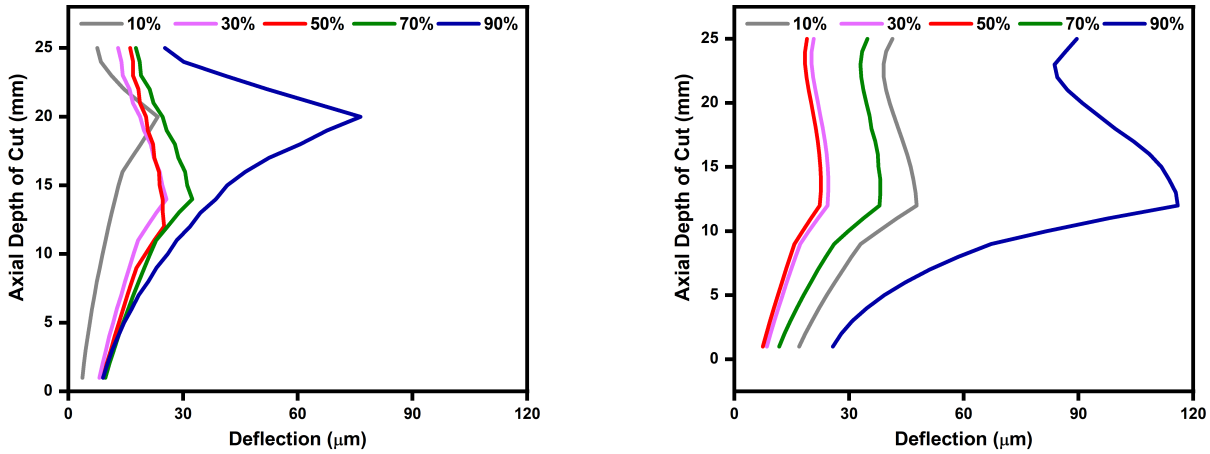

(a) With RRA Algorithm **(b)** With Constant *RDOC*

Figure 5.16 : Axial Surface Error Variation along Length of Component for Circular Convex Component

Figure 5.17a and 5.17b depicts the graphical representation of machined surface as well as cylindricity parameters obtained using the RRA and constant *RDOC* approach along with experimental results. The cylindricity error is considerably reduced for workpiece geometry obtained using RRA as the magnitude of minimum and maximum distortion is reduced

significantly. The RRA exploits size of the mating envelopes as a governing element to control the tolerance zone in this case. The magnitude of geometric tolerance is optimized by regulating the radius of the enveloping coaxial cylinders. It is observed that the radius of the mating cylinders connecting the nearest and farthest distorted coordinates is minimized for the case of convex geometries. The change in the radius of bounding cylinders was captured by computational models effectively and the same is summarized in Table 5.4.

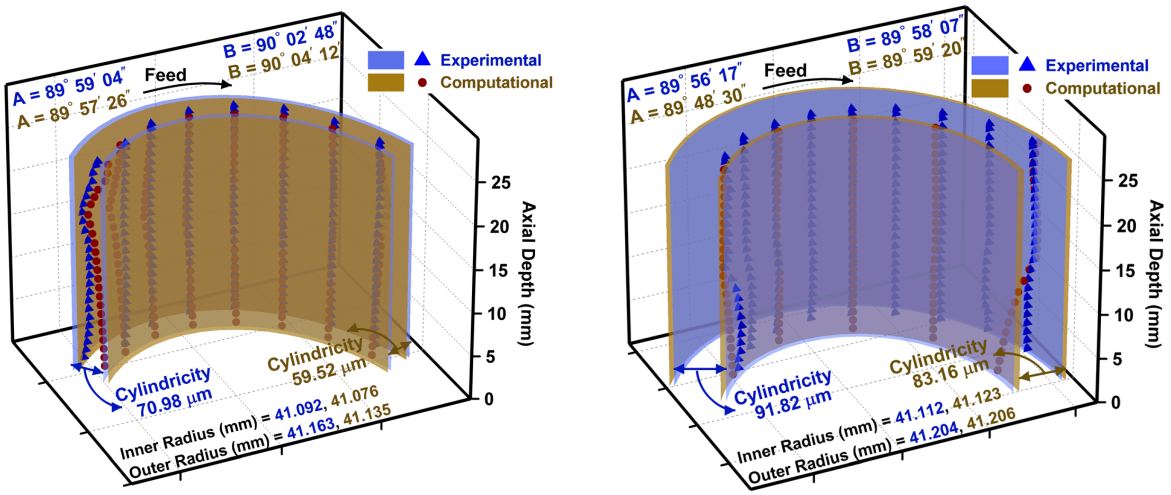

(a) With RRA Algorithm

(b) With Constant *RDOC*

Figure 5.17 : Cylindricity Profile and associated Parameters for Circular Convex Component

5.5 SUMMARY

This chapter presented a novel approach to control geometric tolerances during end milling of thin-walled straight and circular components. The algorithm considers the final geometric configuration of the workpiece as an input and proposes to generate a semi-finished workpiece geometry such that the geometric tolerances are optimized while performing finish cutting sequence. The objective is accomplished by employing the PSO technique to regulate the rigidity of thin-walled component and determines variation of *RDOC* along the length of the component. It was observed that the proposed approach can effectively manipulate the combination of three independent governing parameters controlling geometric tolerances namely, size of the mating envelopes, orientation of the bounding feature and position of the reference feature. This has been validated by employing the algorithm for thin-walled geometries having straight, concave and convex configuration in determining regulated semi-finishing geometries. The effectiveness of the proposed algorithm is substantiated further by conducting a set of end milling experiments for each of these cases. The results obtained by implementing proposed strategy are compared with a traditional approach considering constant *RDOC* value along the length of the cut. The outcomes presented in this chapter demonstrated that the RRA has great potential to optimize geometric tolerances during machining of thin-walled geometries.

...